www.czasopisma.pan.pl PAN www.journals.pan.pl
Opto-Electronics Review 25 (2017) 205–208

Contents lists available at ScienceDirect

Opto-Electronics Review

journal homepage: http://www.journals.elsevier.com/opto-electronics review

High peak power 16 μm InP-related quantum cascade laser

A. Szerling[a,*], S. Slivken[b], M. Razeghi[b]

[a] Instytut Technologii Elektronowej, Al. Lotników 32/46, 02-668 Warsaw, Poland
[b] Center for Quantum Devices, 2220 Campus Drive Cook Hall, Northwestern University, Evanston, IL 60208-0893, United States

ARTICLE INFO

Article history:
Received 16 January 2017
Received in revised form 30 May 2017
Accepted 13 June 2017
Available online 22 July 2017

Keywords:
Quantum cascade lasers
SiO_2 layer
InP

ABSTRACT

In this paper ~16 μm-emitting multimode InP-related quantum cascade lasers are presented with the maximum operating temperature 373 K, peak and average optical power equal to 720 mW and 4.8 mW at 303 K, respectively, and the characteristic temperature (T_0) 272 K. Two types of the lasers were fabricated and characterized: the lasers with a SiO_2 layer left untouched in the area of the metal-free window on top of the ridge, and the lasers with the SiO_2 layer removed from the metal-free window area. Dual-wavelength operation was obtained, at $\lambda \sim 15.6\,\mu m$ (641 cm^{-1}) and at $\lambda \sim 16.6\,\mu m$ (602 cm^{-1}) for lasers with SiO_2 removed, while within the emission spectrum of the lasers with SiO_2 left untouched only the former lasing peak was present. The parameters of these devices like threshold current, optical power and emission wavelength are compared. Lasers without the SiO_2 layer showed ~15% lower threshold current than these ones with the SiO_2 layer. The optical powers for lasers without SiO_2 layer were almost twice higher than for the lasers with the SiO_2 layer on the top of the ridge.

1. Introduction

Quantum cascade lasers (QCLs) are unipolar sources of coherent radiation known since 1994 [1], with operation based on tunneling transport of carriers and intersubband optical transitions. They may be fabricated on the basis of many different types of epitaxial semiconductor structures, though mainly based on III–V materials. QCLs' operating wavelengths span both mid-infrared (MIR) and far-infrared regions, with the exception of the reststrahlen band which for III–Vs lies in the 20–60 μm range. Among the III–V-related QCLs the InP-based ones proved to be particularly effective sources of radiation both in MIR [2–4] and THz region [2,5–7]. The QCLs emitting in MIR wavelength range up to 12 μm are effective radiation sources, perfectly matching the requirements of gas detection systems [8]. However, for longer wavelengths, i.e., when we move toward the reststrahlen region, the QCLs' technology is more and more demanding. Only recently, the room-temperature continuous-wave 15-μm-emitting InAs-based QCLs have been presented by Baranov et al. [9]. Generally, however, for 12–20 μm wavelengths only limited performance has been demonstrated for high power QCL operation at room temperature, despite the existing strategic application areas [10]. In particular, in the 12–16 μm wavelength region, large organic hydrocarbon molecules like the BTX aromatic compounds (benzene, toluene and isomers of xylene) [11], that are very important for petroleum refining and petrochemical industries [8], can be detected. Longer-wavelength sources would also be valuable for radio-astronomy as local oscillators in heterodyne detectors [8].

2. Experimental work

This paper deals with $\lambda \sim 16\,\mu m$-emitting InP-related QCLs operating at room temperature. Its InGaAs/InAlAs structure, which is based on a bound-to-continuum design, generally follows the construction by Rochat et al. [8]. The InP-related structure was grown by gas-source molecular-beam epitaxy and consists of a 45-period InGaAs/InAlAs active region embedded in an optical waveguide which relies on dielectric confinement, with air or vacuum acting as an upper cladding. The long-wavelength radiation is seriously absorbed by free carriers, and that is why the surface-plasmon waveguide is not an effective solution in this case. The waveguide consists of two low Si-doped ($n = 6 \times 10^{16}\ cm^{-3}$) InGaAs guiding layers grown below and above the active region, with thicknesses of 600 nm and 1750 nm, respectively. Electrical injection in the structure is obtained laterally through a heavily Si-doped ($n = 1 \times 10^{18}\ cm^{-3}$) 600 nm-thick InGaAs contact layer.

The devices were processed in 50 μm to 70 μm-wide double-trench mesas using wet chemical etching and a SiO_2 layer for passivation and isolation. The evaporated top metallization consisted of Ti/Au (40/120 nm), and a 3 μm-thick electroplated gold

* Corresponding author.
E-mail address: szerling@ite.waw.pl (A. Szerling).

http://dx.doi.org/10.1016/j.opelre.2017.06.007
1896-3757/

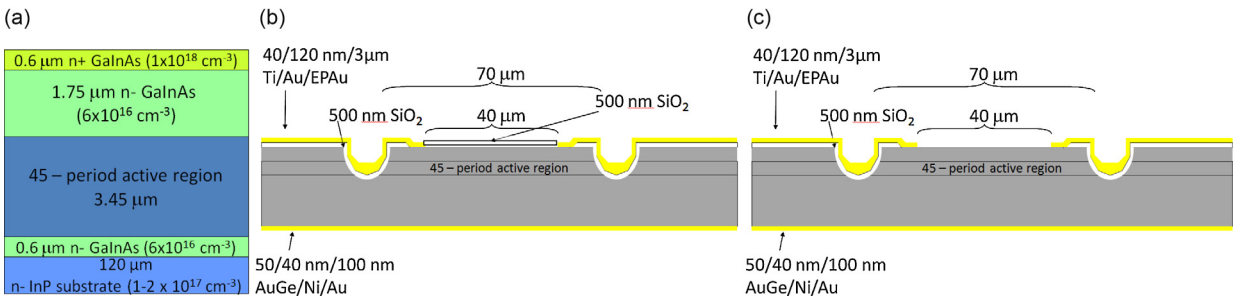

Fig. 1. (a) A schematic of the laser semiconductor structure that was fabricated into lasers A and B. (b), (c) Schematic views of lasers A and B, respectively, with ridge widths of 70 µm. Layer thicknesses are not to scale.

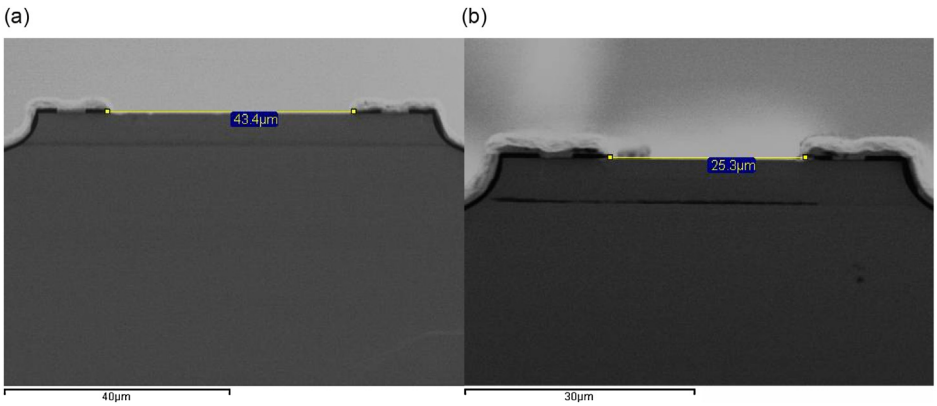

Fig. 2. Representative SEM images of the mirror-sides of the fabricated ~16 µm-emitting lasers B with 70 µm-wide ridges (a) and 50 µm-wide ridges (b), with measured exact widths of the prepared metal-free windows.

layer was deposited on it for better heat removal. The top contacts area was restricted to the edges of the ridge only, and the main part of the ridge surface was left free of metallic layer. Calculations show there is a threefold increase of absorption losses when a continuous metal layer is present on top of the ridge [12]. The widths of the metal-free windows were 25 µm and 40 µm for the 50 µm-wide and 70 µm-wide ridges, respectively. The back contact consisted of AuGe/Ni/Au (50/40/100 nm) metallization deposited on a thinned InP substrate. The wafers were cleaved into laser bars with a 2 mm cavity length in a direction normal to the cleaved mirrors and indium soldered to copper heat sinks with the epilayer side up. The device packaging was finished by the gold wire bonding for the top contact. The lasers' mirror remained uncoated. In this work we were focused on presenting the maximum emitted optical powers for this type of laser, that is why only the results for 70 µm-wide lasers are shown in the paper.

Two types of such devices were examined by us: the lasers with the SiO_2 layer left untouched in the area of the metal-free window on top of the ridge (lasers A) and the lasers with the SiO_2 layer removed from the metal-free window area (lasers B). Fig. 1 presents design details of the lasers A and B with 70 µm-wide ridges.

In Fig. 2, the scanning electron microscopy (SEM) images of the lasers B with two different ridge widths are presented.

For L–I–V characteristics and spectrum measurements, a pulse width in the range 100–300 ns and a duty cycle in the range 0.5–1.8% were used. Temperature dependent power measurements were carried out on a thermoelectric cooler stage using a calibrated thermopile placed directly below the copper table on which the heatsinks with lasers were mounted. In the text and figures below, the peak (P_{peak}) and average (P_{av}) powers are given per one mirror.

Though it is technologically easier to leave the SiO_2 layer untouched, it is known that it is strongly absorbing material in the long wavelength infrared region. Indeed, lasers B, in comparison with lasers A, proved to have better performance, in terms of threshold current density, output power and slope efficiency. We measured several lasers of these two types and their described behaviour was repeatable.

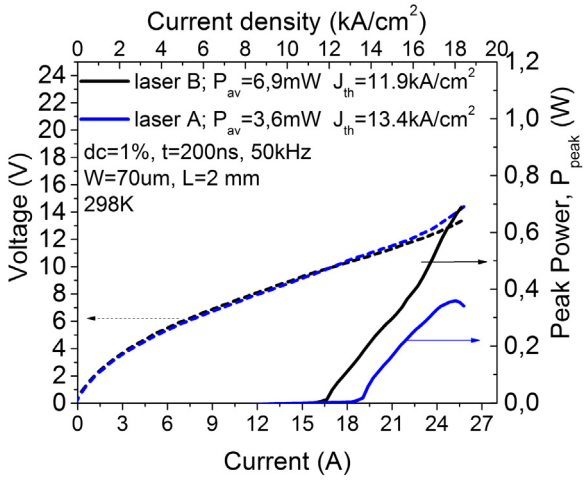

Fig. 3. Representative L–I–V characteristics for the lasers A (blue line) and B (black line) with 70 µm-wide ridges measured at 298 K. The average emitted power (P_{av}) was at least 6.9 mW for lasers B (the limit is set here by the current driver) and 3.6 mW for lasers A.

In Fig. 3, there is comparison of L–I–V characteristics measured at the room temperature (298 K) for lasers A and B with 70 µm-wide ridges. The average threshold current density for the lasers B was 15% lower than for the lasers A. What is more each individual laser B had lower threshold current density than any one of the lasers A. Also, while the average output power for a set of lasers A was only ~3.6 mW, the average optical power for lasers B was almost

twice higher. There was not found any laser A with output power higher than the power for any one of the lasers B. The lasers with the SiO_2 layer removed from the metal-free window area showed ~20% higher slope efficiencies than these ones with SiO_2 layer left on the metal-free window area, which can be calculated for the representative light-current characteristics presented in Fig. 3 in the paper. The slope efficiencies of the two types of the lasers are initially, for lower feeding currents, of very similar value and start to differ strongly mainly at higher currents.

It has to be emphasized, we have not observed Stark-effect rollover in any laser tested by us. Therefore, we believe that overheating of the laser's active region is a very probable reason of the optical output-power rollover seen for example in the L–I characteristics presented in Fig. 3, which is representative for the lasers with not removed SiO_2 layer. The overheating may be caused by decreased heat dissipation from the laser ridge induced by additional thermal resistance generated by the left untouched SiO_2 layer. It should be noted here, there is no sharp kink observed in the respective I–V characteristic of the laser A in Fig. 3, like it would be expected in the case of a Stark-effect rollover. It can be mentioned that a similar thermal rollover of the output power can be observed also for the laser B driven with the highest duty cycle, like it is clearly seen in Fig. 5c, while for most measurements of lasers B it was impossible to observe any power rollover effect just for technical reason, i.e., because of the limited current range of the current supplier. However, we take into account that the lower slope (differential) efficiency of the lasers A could additionally be caused by higher optical losses for the lasers with the SiO_2 layer left on the metal-free window area. It should be mentioned here, we have not observed dual-wavelength laser operation for lasers A, i.e., each laser B had always two peak emission, while each laser A had always one peak emission – we will come back to this topic below.

Fig. 4 presents the representative temperature dependence of L–I–V characteristics for the laser B with 70 μm-wide ridge. Its calculated characteristic temperature (T_0) was 272 K and it is clearly

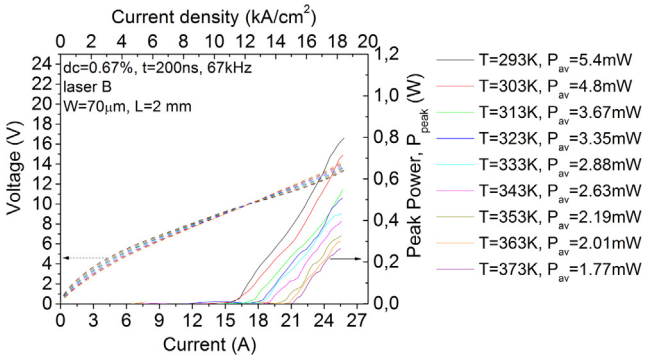

Fig. 4. A set of L–I–V characteristics for a 70 μm-wide ridge laser B measured at different temperatures.

seen in the figure that the maximum operating temperature was over 373 K. The peak power for pulsed operation was up to 700 mW at 303 K, and above 200 mW at 373 K.

The lasers B were also characterized at different supply conditions at the temperature 293 K (Fig. 5a) and at 333 K (Fig. 5b). The average power for 1.8% duty cycle was 3.7 mW at 293 K and 1.62 mW at 333 K. A dependence of average output power on the pulse length, at 298 K, is seen in Fig. 5c.

It was experimentally found that the emission spectra of lasers A emitted single peak only, concentrated around 15.5 μm (Fig. 6a). Under all considered currents and all modulation regimes lasers A emit the single cluster of peaks (with the onset at 641 cm^{-1}). The single-peak emission was also a feature of lasers presented by Rochat et al. [8]. The emission spectra of lasers B is different, as it consists of two clusters of peaks around 15.6 μm (641 cm^{-1}) and ~16.6 μm (602 cm^{-1}). A representative spectrum is shown in Fig. 6b. The emission maxima observed within the spectra of the lasers B are separated by ~39 cm^{-1} because the gain curve of the device is broad enough, i.e., it is more than 40 cm^{-1} [8].

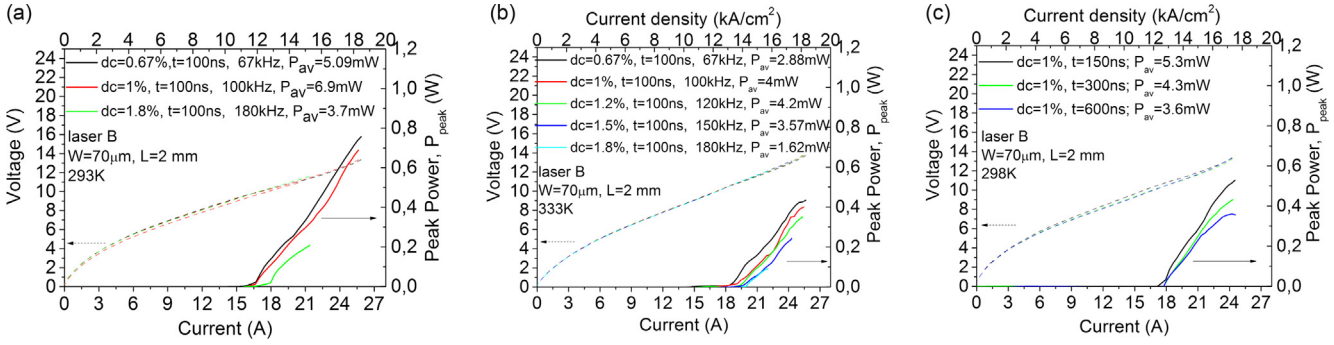

Fig. 5. A set of L–I–V characteristics for laser B with 70 μm-wide ridge measured at different duty cycle at 293 K (a) and 333 K (b), and for different pulse width (c).

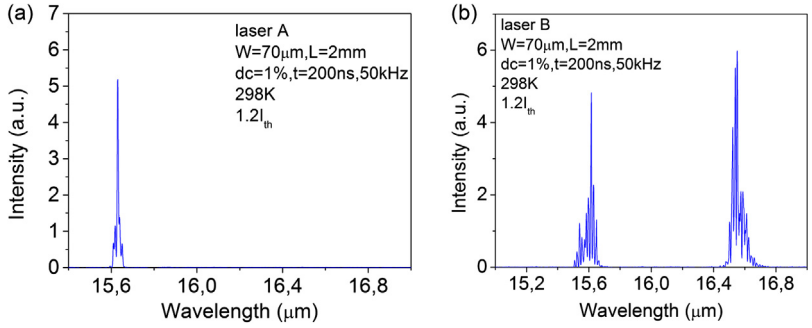

Fig. 6. The lasing spectrum for laser A (a) and laser B (b), with 70 μm-wide ridges.

It is well known that a SiO_2 insulation layer generates increased losses for long wavelength ($\lambda > 13\,\mu m$) lasers [13]. Also, the observed not-existence of two lasing emission peaks in lasers with the remained SiO_2 layer we explain as a result of the absorbing properties of the SiO_2 insulation layer deposited by us. Generally, the SiO_2 layer can absorb the IR radiation including the wavelengths corresponding with our laser's mode peaks. What is more it can be found in a couple of publications that the shape of absorption spectrum of a concrete SiO_2 layer may depend on conditions in which the SiO_2 layer was deposited [14–16] and, hence, the SiO_2 absorption spectrum features can be different for SiO_2 layers obtained in different ways. Here, we put the hypothesis that in our case the SiO_2 layer exhibited much stronger absorption for the wavelength ~16.6 μm than for the wavelength ~15.6 μm, eventually causing that the former peak was totally suppressed in lasers A, while still present in their counterparts without the tight SiO_2 layer.

In contrast to the previous work presented by Rochat et al. [8] in our lasers SiO_2 layer was used as a passivation layer. On the other hand, there is no information if the passivation layer (hard baked resist) used by Rochat et al. [8] was finally removed from top of the ridge. So the possible reason of better performance of the lasers fabricated by us is the explained above concrete fabrication approach.

3. Conclusions

In conclusion, ~16 μm-emitting multimode InP-related quantum cascade lasers are presented with the maximum operating temperature 373 K, peak optical powers 720 mW (303 K), average optical powers 4.8 mW (303 K) and characteristic temperature (T_0) 272 K. Additionally, dual-wavelength operation was obtained, at $\lambda \sim 15.6\,\mu m$ (641 cm^{-1}) and at $\lambda \sim 16.6\,\mu m$ (602 cm^{-1}), however, only for the lasers with the SiO_2 layer removed from the metal-free window area. The lasers with the removed SiO_2 layer showed ~15% lower threshold current than these ones with a SiO_2 layer left on the metal-free window area. At the same time, while the average output power for a set of lasers with SiO_2 layer on the metal-free window area was only ~3.6 mW, the optical powers for lasers without SiO_2 layer on the metal-free window area were almost twice higher (at 298 K). We believe the performance improvement in comparison with the lasers with the SiO_2 layer is mainly a result of changed laser technology. In our opinion, the crucial was removal of SiO_2 layer from the top area of the ridge, from between the metallic contacts – that removal has likely resulted in the enhanced heat dissipation from the active region, blocked earlier by the SiO_2 layer and/or in the reduced absorption losses assumedly generated by the oxide.

Acknowledgements

Anna Szerling would like to thank Kamil Kosiel, Ph.D., D.Sc. (from Instytut Technologii Elektronowej, Warsaw, Poland) for the fruitful discussion. The work was in part financially supported by project LIDER/34/70/L-3/11/NCBR/2012 by the Polish National Center for Research and Development. Dr Anna Szerling was supported by COST ACTION MP1204 TERA-MIR Radiation: Materials, Generation, Detection and Applications.

References

[1] J. Faist, F. Capasso, D.L. Sivco, C. Sirtori, A.L. Hutchinson, A.Y. Cho, Quantum cascade laser, Science 264 (5158) (1994) 553–556.
[2] M. Razeghi, Q.Y. Lu, N. Bandyopadhyay, W. Zhou, D. Heydari, Y. Bai, S. Slivken, Quantum cascade lasers: from tool to product, Opt. Express 23 (2015) 8462–8475.
[3] Y. Bai, S. Slivken, S.R. Darvish, M. Razeghi, Room temperature continuous wave operation of quantum cascade lasers with 12.5% wall plug efficiency, Appl. Phys. Lett. 93 (2) (2008).
[4] M. Razeghi, N. Bandyopadhyay, Y. Bai, Q. Lu, S. Slivken, Recent advances in mid infrared (3–5 μm) quantum cascade lasers, Opt. Mater. Express 3 (2013) 1872–1884.
[5] Q.Y. Lu, N. Bandyopadhyay, S. Slivken, Y. Bai, M. Razeghi, Room temperature single-mode terahertz sources based on intracavity difference-frequency generation in quantum cascade lasers, Appl. Phys. Lett. 99 (13) (2011) 131106.
[6] Q.Y. Lu, N. Bandyopadhyay, S. Slivken, Y. Bai, M. Razeghi, Widely tuned room temperature terahertz quantum cascade laser sources based on difference-frequency generation, Appl. Phys. Lett. 101 (25) (2012) 251121.
[7] Q. Lu, M. Razeghi, Recent advances in room temperature, high-power terahertz quantum cascade laser sources based on difference-frequency generation, Photonics 3 (3) (2016) 42.
[8] M. Rochat, D. Hofstetter, M. Beck, J. Faist, Long-wavelength ($\lambda \approx 16\,\mu m$), room-temperature, single-frequency quantum-cascade lasers based on a bound-to-continuum transition, Appl. Phys. Lett. 79 (2001) 4271–4273.
[9] A.N. Baranov, M. Bahriz, R. Teissier, Room temperature continuous wave operation of InAs-based quantum cascade lasers at 15 μm, Opt. Express 24 (16) (2016) 18799–18806.
[10] M.S. Vitiello, G. Scalari, B. Williams, P. De Natale, Quantum cascade lasers: 20 years of challenges, Opt. Express 23 (4) (2015) 5167–5182.
[11] J. Faist, D. Hofstetter, M. Beck, T. Aellen, M. Rochat, S. Blaser, Bound-to-continuum and two-phonon resonance, quantum-cascade lasers for high duty cycle, high-temperature operation, IEEE J. Quantum Electron. 38 (6) (2002) 533–546.
[12] S. Slivken, Private communication.
[13] X. Huang, Y. Chiu, W.O. Charles, C. Gmachl, Ridge-width dependence of the threshold of long wavelength ($\lambda \approx 14\,\mu m$) quantum cascade lasers with sloped and vertical sidewalls, Opt. Express 20 (3) (2012) 2539–2547.
[14] C.E. Viana, A.N.R. da Silva, N.I. Morimoto, O. Bonnaud, Analysis of SiO_2 thin films deposited by PECVD using an oxygen-TEOS-argon mixture, Braz. J. Phys. 31 (2) (2001), São Paulo.
[15] S.C. Deschmukh, E.S. Aydil, Investigation of low temperature SiO_2 plasma enhanced chemical vapor deposition, J. Vac. Sci. Technol. B 14 (1996) 738.
[16] S.K. Ray, C.K. Maiti, S.K. Lahiri, N.B. Chafrabarti, Properties of silicon dioxide films deposited at low temperatures by microwave plasma enhanced decomposition of tetraethylorthosilicate, J. Vac. Sci. Technol. B 10 (1992) 1139.